



DEVELOPMENT OF NOVEL AND COST-EFFECTIVE CORROSION RESISTANT COATINGS
FOR HIGH TEMPERATURE GEOTHERMAL APPLICATIONS

| | | | |
|-------------------------|---|----------------------------|--------------------|
| Project acronym: | Geo-Coat | | |
| Project title: | Development of Novel and Cost-Effective Corrosion Resistant Coatings for High Temperature Geothermal Applications | | |
| Activity: | LCE-07-17-Renewables | | |
| Call: | H2020-LCE-2017-RES-RIA-TwoStage | | |
| Funding Scheme: | RIA | Grant Agreement: | LCE-GA-2018-764086 |
| Project dates: | 01/02/2018 – 31/01/2021 | Duration in months: | 36 |
| WP3 | Coating synthesis through thermal spray and laser cladding | | |

D3.6: Phase transformation rules to apply heat treatment during HEA coating synthesis

| | | | |
|---|-------------------------------------|----------------------------------|--|
| Due date: | 31/03/2019 (M14) | | |
| Actual Submission Date: | 29/03/2019 | | |
| Lead Beneficiary: | University "Politehnica" Bucharest | | |
| Main authors/contributors: | UPB, MET, TEH, TWI | | |
| Dissemination Level¹: | PU | | |
| Nature: | Report | | |
| Status of this version: | <input type="checkbox"/> | Draft under Development | |
| | <input type="checkbox"/> | For Review by Coordinator | |
| | <input checked="" type="checkbox"/> | Submitted | |
| Version: | 02 | | |

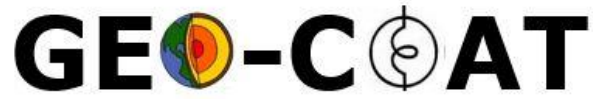
REVISION HISTORY

| Version | Date | Main Authors/Contributors | Description of changes |
|---------|------------|------------------------------------|---|
| 02 | 30/07/2019 | University "Politehnica" Bucharest | Updated with latest available technical information |
| | | | |
| | | | |

¹ Dissemination level security:

PU – Public (e.g. on website, for publication etc.) / PP – Restricted to other programme participants (incl. Commission services) /

RE – Restricted to a group specified by the consortium (incl. Commission services) / CO – confidential, only for members of the consortium (incl. Commission services)



DEVELOPMENT OF NOVEL AND COST-EFFECTIVE CORROSION RESISTANT COATINGS
FOR HIGH TEMPERATURE GEOTHERMAL APPLICATIONS



Funded by the Horizon 2020
Framework Programme of the
European Union



DEVELOPMENT OF NOVEL AND COST-EFFECTIVE CORROSION RESISTANT COATINGS
FOR HIGH TEMPERATURE GEOTHERMAL APPLICATIONS

This project has received funding from the European Union's Eighth Framework Programme for research, technological development and demonstration under Grant Agreement No. LCE-GA-2018-764086. This publication reflects the views only of the author(s), and the Commission cannot be held responsible for any use which may be made of the information contained therein.

Copyright © 2018-2021, Geo-Coat Consortium

This document and its contents remain the property of the beneficiaries of the Geo-Coat Consortium and may not be distributed or reproduced without the expressed written approval of the Geo-Coat Coordinator, TWI Ltd. (www.twi-global.com)

THIS DOCUMENT IS PROVIDED BY THE COPYRIGHT HOLDERS AND CONTRIBUTORS "AS IS" AND ANY EXPRESS OR IMPLIED WARRANTIES, INCLUDING, BUT NOT LIMITED TO, THE IMPLIED WARRANTIES OF MERCHANTABILITY AND FITNESS FOR A PARTICULAR PURPOSE ARE DISCLAIMED. IN NO EVENT SHALL THE COPYRIGHT OWNER OR CONTRIBUTORS BE LIABLE FOR ANY DIRECT, INDIRECT, INCIDENTAL, SPECIAL, EXEMPLARY, OR CONSEQUENTIAL DAMAGES (INCLUDING, BUT NOT LIMITED TO, PROCUREMENT OF SUBSTITUTE GOODS OR SERVICES; LOSS OF USE, DATA, OR PROFITS; OR BUSINESS INTERRUPTION) HOWEVER CAUSED AND ON ANY THEORY OF LIABILITY, WHETHER IN CONTRACT, STRICT LIABILITY, OR TORT (INCLUDING NEGLIGENCE OR OTHERWISE) ARISING IN ANY WAY OUT OF THE USE OF THIS DOCUMENT, EVEN IF ADVISED OF THE POSSIBILITY OF SUCH DAMAGE.

SUMMARY

In this deliverable we present the work performed to develop the phase transformation rules to be applied for HEA coating synthesis. The corrosion behaviour of high-entropy alloy coatings has in fact a close relationship with the properties of the passive film which develops on the coating surface. The properties of this latter can be altered by heat treatment of the system before exposure to the corrosion environment. A comprehensive study of the microstructural properties of the passive film, its modifications after heat treatment and its effect on the corrosion performance of the produced coatings has been performed within the project. While the in-depth characterisation of the passive film is the focus of deliverable D3.5 (Influence of passive film on the corrosion behaviour of the HEA coating), this deliverable will focus on the phase transformations observed during the study and on the effect onto the corrosion performance of the coatings. For this reason, in this deliverable, new specimens have been produced at the same conditions of the optimised HEA coated substrates obtained from Task 3.3 and Task 3.4 (whose corrosion and erosion behaviour has been evaluated in the as-deposited condition). The as-deposited specimens have been then heat-treated and then their corrosion behaviour re-investigated and compared to previous results on the as-deposited specimens. Three heat-treatment factors such as heating rate, cooling rate and time have been considered, as originally established in the DoE in deliverable D3.1 (Adaptive DOE for optimisation of laser cladding and HVOF process). Both equilibrium and non-equilibrium thermodynamics calculations have been performed in this deliverable to predict the phase formation/transformation.

In this report, after a first section focusing on the design and characterisation of the powders used to deposit the coatings, the effect of heat treatment on the phase and corrosion behaviour of the deposited coatings (produced through HVOF and laser cladding) is presented. Results from this deliverable will help develop the phase-formation rules under both equilibrium and non-equilibrium conditions to guide the heat treatment and coating processes.

Objective Met

The following objectives have been met:

- To study and categorise the chemistry/physics of the HEA passive films and the effects of heat treatment and consolidation on the density and porosity, hence corrosion and erosion resistance, of HEA coatings.

Document: D3.6 : Scientific study on the passive film and heat treatment on corrosion behaviour of HEAs
Version: 01
Date: 31 July 2019

CONTENTS

| | |
|--|----|
| SUMMARY | 4 |
| OBJECTIVE MET..... | 4 |
| 1. MATERIALS AND SETUP | 6 |
| 2. METHODOLOGY..... | 7 |
| 2.1 METHODOLOGY FOR HEA POWDER DESIGN..... | 7 |
| 2.2 METHODOLOGY FOR COATINGS DEPOSITION AND HEAT TREATMENT | 10 |
| 3. RESULTS | 11 |
| 3.1 HEA POWDERS CHARACTERISATION | 11 |
| 3.2. PERFORMANCE AND CHARACTERISATION OF HEAT TREATED COATINGS..... | 14 |
| 3.2.1. <i>HVOF coatings – characterisation of heat treatment</i> | 14 |
| 3.2.2. <i>Effect of heat treatment on corrosion performance</i> | 16 |
| 3.2.3. <i>LMD coatings – characterisation of heat treatment</i> | 17 |
| 3.2.4. <i>LMD coatings – effect of heat treatment on corrosion performance</i> | 19 |
| 4. DISCUSSION – PHASE EVOLUTION DURING HEAT TREATMENT | 20 |
| 5. CONCLUSION | 24 |
| REFERENCES..... | 24 |

1. MATERIALS AND SETUP

The powders used to produce the coatings in this section are custom made high-entropy alloys (HEA) produced by either mechanical alloying or gas atomisation: HEA 1 – CoCrFeNiMo_{0.85}, HEA 3 – CoCrFeNiMo, HEA 4 – Co_{0.5}CrFeNiMo, HEA 5 – Al_{0.5}CoCrFeNi, HEA 6 – HfNbTaTiZr. Details on their production methodology and final microstructure has been reported in deliverable D3.2. (Report on optimisation of HVOF process for HEA and cermet alloy based coating synthesis). As also described in this deliverable, one set of deposition process parameters has been employed to produce the coatings as a result of the optimisation stage. This optimum set of process parameters (one per powder) has been employed to produce the specimens in this stage by only employing either carbon steel (substrate S1 within Geo-Coat for laser cladding specimens) or stainless steel (substrate S4 within Geo-Coat for HVOF specimens) as substrates of dimensions of 25x25x6 mm. Details on powders, deposition process parameters optimisation and setup used for HVOF and laser cladding are presented in deliverables D3.2 (for HVOF) and D3.3 (for laser cladding).

The furnace employed for the heat-treatment runs in this stage is an L laboratory chamber furnace (LAC®), capable of operating in AR atmosphere up to a temperature of 1200 °C (Fig. 1).



Figure 1: Furnace used for heat treatment of the HEA coated samples

A Field Emission Scanning Electron Microscope (SEM Supra 25, Zeiss®), equipped with X-Ray Energy Dispersive Spectroscopy (EDS, Oxford instruments®) equipment was employed to evaluate the coatings microstructure. For these analyses, the specimens were cross-sectioned and mounted in a thermosetting phenol formaldehyde resin (Bakelite) and ground and polished with SiC abrasive paper. X-ray Diffraction data for phase characterisation of both powders and coatings has been collected by using a Bruker D8 advance instrument equipped with a Cu target X-ray tube and a diffracted beam monochromator limiting the beam to Cu K α radiation. Data was collected between $2\theta = 15^\circ$ and 90° at 0.05° intervals.

The corrosion performance of both as-sprayed and heat-treated coatings has been examined in a 3.5% NaCl aqueous solution at room temperature (25°C) and constant pH = 4. The pH was controlled by means of an HCl 7.5M solution during the experiments. Saturated calomel electrode (SCE) and platinised titanium electrode have been used as reference and auxiliary (counter) electrode respectively. Specimens for corrosion experiments were tested in the as-deposited or as-heat-treated

condition and sealed using epoxy resin, leaving an area of approximately 1 cm² exposed to the solution. The experimental setup of the electrochemical corrosion apparatus was in compliance with ASTM G5-14, ASTM G59-97. The electrochemical properties of the specimens were assessed experimentally by potentiodynamic polarisation resistance and Tafel scan measurements following ASTM G102-89. All potentiodynamic polarisation measurements were taken using an ACM Instruments® Gill 16 electrochemical system, while a Bank Elektronik GmbH® Azelle 5 avesta cell was employed for the Tafel scans. Potentiodynamic polarisation measurements were taken at -/+ 10 mV versus the corrosion potential, with a scanning rate of 10 mV/min and a total testing time of 1 week. Tafel scan measurements were taken from -250 mV to + 150 mV versus open-circuit potential (E_{OCP}) at a scanning rate of 0.5 mV/s by first keeping the working electrode immersed into the test solution at E_{OCP} for 60 min to attain a steady-state condition. Results were analysed by using the ACM® Core Running software. An in depth description of the electrochemical equipment is provided in deliverable D5.3 (Ranking of the synthesised coatings).

2. METHODOLOGY

In this section, the methodology employed for the design of the powders, the coatings heat-treatments and their analysis is reported.

2.1 Methodology for HEA powder design

The 11 compositions of high entropy alloys have been designed and down selected according to theoretical calculations. From previous research, leading to the ideas developed in Geo-Coat, it was shown that the composition CoCrFeNiMo performed well in geothermal steam [1]. This combination of elements (Co_xCrFeNiMo_y) was thus employed and investigated together with two other composition classes: Al_xCoCrFeNi and HfNbTa_xTiZr, due to their potentially good corrosion and erosion performance.

A solid solution formation parameter, Ω , was calculated to predict the solid solution phase formation. The solid solution formation parameter is defined as:

$$\Omega = \frac{T_m \Delta S_{mix}}{\Delta H_{mix}} \quad (1)$$

where the entropy of mixing is:

$$\Delta S_{mix} = -R \sum_{i=1}^n c_i \ln c_i \quad (2)$$

and R is the gas constant. The enthalpy of mixing is

$$\Delta H_{mix} = \sum_{i=1, i \neq j}^n \Omega_{ij} c_i c_j \quad (3)$$

where $\Omega_{ij} = 4\Delta_{mix}^{AB}$, Δ_{mix}^{AB} is the mixing enthalpy of binary liquid AB alloys. Another important parameter is the atomic size difference, given by:

$$\delta = \sqrt{\sum_{i=1}^n c_i (1 - \frac{r_i}{\bar{r}})} \quad (4)$$

where $\bar{r} = \sum_{i=1}^n c_i r_i$, c_i and r_i are the atomic percentage and atomic radius of the i^{th} element respectively.

According to the criteria of phase stability formation calculated by Zhang et al. [2], if $\Omega \geq 1.1$ and $\delta \leq 6.6$ then the solid solution forms. Takeuchi et al. [4] studied the effects of changes in the mixing entropy, ΔS_{mix} , to the crystal structure formation, their findings suggest that the higher the mixing entropy, the more confused the system gets when trying to form an ordered structure. Thus, the mixing entropy reflects the system complexity. The valence electron concentration (VEC) plays a decisive role in determining whether face-centred cubic (FCC) or body-centred cubic (BCC) crystal structure solid solution forms in HEAs. Specifically, larger VEC (≥ 8) favours the formation of FCC-type solid solutions, while smaller VEC (< 6.87) favours the formation of BCC-type solid solutions according to Guo et al. [3]. The total valence electron concentration is given by:

$$VEC = \sum_{i=1}^n c_i VEC_i \quad (5)$$

where VEC_i is the valence electron concentration of each component and c_i is the concentration of each component of the high entropy alloy. The first system were theoretical calculation have been performed was CoCrFeNiMo_x. Therefore, for high-entropy alloys usually the calculation performed are related to Valence Electron Concentration (VEC), ΔS_{mix} (mixing entropy), ΔH_{mix} (mixing enthalpy), Ω (solid solution formation parameter), and T_m (melting temperature).

Within the Geo-Coat project, the above described parameters have been calculated for a range of compositions (varying from 0 to 2 in molar ratio) based on the three material classes Co_xCrFeNiMo, Al_xCoCrFeNi and HfNbTa_xTiZr. Among the tested compositions, the ones where VEC value between 6.87 and 8 have been selected, in order to have a mixture of FCC + BCC phases providing the necessary properties combination for the coating to be extremely resistant in geothermal environment. In fact, the FCC phase is expected to present a ductile nature while the opposite holds for a BCC crystal structure. It is thus expected that a mixed FCC+BCC microstructure would provide the benefits in terms of tribological properties (e.g. resistance to erosion wear).

The calculated thermodynamic parameters for compositions CoCrFeNiMo_x, Co_xCrFeNiMo, Al_xCoCrFeNi and HfNbTa_xTiZr are reported in Tabs. 1-4. In the same tables, the selected compositions have been highlighted. The compositions were selected according to their theoretical properties. A VEC of approximately 7.8 is considered favourable, to increase the FCC amount. To ensure the composition remains within the high entropy alloys domain, variation of the entropy, ΔS , enthalpy, ΔH_{mix} , and atomic size difference, δ , have to be between the following limits:

$$-22 \leq \Delta H_{mix} \leq 7$$

$$11 \leq \Delta S_{mix} \leq 19.5$$

$$0 \leq \delta \leq 8.5$$

For all the selected alloys, it was determined that VEC between 7.68 – 7.8 would provide the most suitable corrosion behaviour. The intent was to avoid brittle phase. The only exception was made for the HfNbTaTiZr high entropy alloy whose VEC is 3.4 and is prone to form BCC single solid solution. This last alloy presents additional challenges, but was considered of interest for testing in geothermal environment to observe its properties in this highly aggressive environment.

Table 1: Theoretical calculation for parameters characterizing HEA for the composition CoCrFeNiMo_x

| | CoCrFeNiMo ₀ | CoCrFeNiMo _{0.5} | CoCrFeNiMo | CoCrFeNiMo _{1.5} | CoCrFeNiMo _{0.85} | CoCrFeNiMo ₂ |
|-----|-------------------------|---------------------------|------------|---------------------------|----------------------------|-------------------------|
| VEC | 8.25 | 8.025 | 7.8 | 7.575 | 7.69 | 7.35 |

Document: D3.6 : Scientific study on the passive film and heat treatment on corrosion behaviour of HEAs
Version: 01
Date: 31 July 2019

| | | | | | | |
|------------------|----------|----------|----------|----------|----------|----------|
| \bar{r} | 1246.75 | 1257.075 | 1267.4 | 1277.725 | 1274.64 | 1288.05 |
| δ | 0.0381 | 0.0194 | 0.0011 | 0.0170 | 0.0116 | 0.0348 |
| χ_b | 1.82 | 1.854 | 1.888 | 1.922 | 1.9149 | 1.956 |
| χ | 0 | 0 | 0 | 0 | 0 | 0 |
| ΔS_{mix} | 11.53 | 13.08 | 13.38 | 13.15 | 10.32 | 12.51 |
| ΔH_{mix} | -0.086 | -0.1719 | -0.1856 | -0.1911 | -0.086 | -0.1884 |
| Tm | 1859.25 | 1962.93 | 2066.60 | 2170.28 | 2134.24 | 2273.95 |
| Ω | 249.1752 | 149.3128 | 148.9919 | 149.3036 | 256.0458 | 151.0030 |

Table 2: Theoretical calculation for parameters characterizing HEA for the composition $\text{Co}_x\text{CrFeNiMo}$

| | $\text{Co}_0\text{CrFeNiMo}$ | $\text{Co}_{0.5}\text{CrFeNiMo}$ | CoCrFeNiMo | $\text{Co}_{1.5}\text{CrFeNiMo}$ | $\text{Co}_2\text{CrFeNiMo}$ |
|------------------|------------------------------|----------------------------------|---------------------|----------------------------------|------------------------------|
| VEC | 6.15 | 7.5 | 7.8 | 7.65 | 7.95 |
| \bar{r} | 1.32085 | 1271.5 | 1267.4 | 1269.45 | 1265.35 |
| δ | 0.4081 | 0.0062 | 0.0011 | 0.0026 | 0.0047 |
| χ_b | 1.736 | 1.89 | 1.888 | 1.889 | 1.887 |
| χ | 0 | 0 | 0 | 0 | 0 |
| ΔS_{mix} | 12.50 | 11.53 | 13.38 | 13.08 | 13.15 |
| ΔH_{mix} | -0.6492 | -0.19 | -0.1856 | -0.1899 | -0.1771 |
| Tm | 1489.15 | 2141.25 | 2066.60 | 2103.93 | 2029.28 |
| Ω | 28.6838 | 129.8911 | 148.9919 | 144.8687 | 150.6394 |

Table 3: Theoretical calculation for parameters characterizing HEA for the composition $\text{Al}_x\text{CoCrFeNi}$

| | $\text{Al}_0\text{CrFeNiCo}$ | $\text{Al}_{0.5}\text{CrFeNiCo}$ | AlCrFeNiCo | $\text{Al}_{1.5}\text{CrFeNiCo}$ | $\text{Al}_2\text{CrFeNiCo}$ |
|------------------|------------------------------|----------------------------------|---------------------|----------------------------------|------------------------------|
| VEC | 8.25 | 7.725 | 7.2 | 6.675 | 6.15 |
| \bar{r} | 1.24675 | 1.265275 | 1.2838 | 1.302325 | 1.32085 |
| δ | 0.51213893 | 0.484997582 | 0.458639523 | 0.433031328 | 0.408141446 |
| χ_b | 1.82 | 1.799 | 1.778 | 1.757 | 1.736 |
| χ | 0 | 0 | 0 | 0 | 0 |
| ΔS_{mix} | 11.52 | 13.07 | 13.37 | 13.14 | 12.50 |
| ΔH_{mix} | -0.15 | -0.3275 | -0.4928 | -0.6459 | -0.6492 |
| Tm | 1859.25 | 1766.73 | 1674.20 | 1581.68 | 1489.15 |
| Ω | 142.7917156 | 70.50465431 | 45.43723441 | 32.17800527 | 28.68377846 |

Table 4: Theoretical calculation for parameters characterizing HEA for the composition $\text{HfNbTa}_x\text{TiZr}$

| | $\text{Ta}_0\text{NbHfZrTi}$ | $\text{Ta}_{0.5}\text{NbHfZrTi}$ | TaNbHfZrTi | $\text{Ta}_{1.5}\text{NbHfZrTi}$ | $\text{Ta}_2\text{NbHfZrTi}$ |
|------------------|------------------------------|----------------------------------|---------------------|----------------------------------|------------------------------|
| VEC | 4.25 | 3.825 | 3.4 | 2.975 | 2.55 |
| \bar{r} | 1.518 | 1.3662 | 1.2144 | 1.0626 | 0.9108 |
| δ | 1.166976111 | 1.365737709 | 1.614189707 | 1.213865473 | 1.639783183 |
| χ_b | 1.4425 | 1.29825 | 1.154 | 1.00975 | 0.8655 |
| χ | 0 | 0 | 0 | 0 | 0 |
| ΔS_{mix} | 11.52 | 13.07 | 13.37 | 13.14 | 12.50 |
| ΔH_{mix} | 0.06 | 0.063 | 0.064 | 29.4336 | 0.06 |
| Tm | 2326.75 | 2121.38 | 1916.00 | 1710.63 | 1505.25 |
| Ω | -446.7401161 | -440.0854744 | -400.3969698 | -0.763692603 | -313.7139351 |

As a result, six compositions have been finally selected, as reported in Table 5. These compositions have been employed to produce the coatings within this report, based on the optimised deposition process parameters reported in deliverable D3.1 and D3.2.

Table 5: Selected composition for high-entropy alloy coatings based on the thermodynamic calculations of tables 1 to 4.

| Composition acronym | Composition |
|---------------------|---|
| HEA 1 | CoCrFeNiMo_{0.85} - mechanically alloyed |
| HEA 2 | CoCrFeNiMo_{0.85} - gas atomised |
| HEA 3 | CoCrFeNiMo |
| HEA 4 | Co_{0.5}CrFeNiMo |
| HEA 5 | Al_{0.5}CoCrFeNi |
| HEA 6* | HfNbTaTiZr |

* To be performed later in the project, after safety tests have been adequately performed.

All of the powders in Table 5 have been then produced through mechanical alloying, with the exception of the powder of composition CoCrFeNiMo_{0.85}, which was produced via both mechanical alloying (HEA 1) and gas atomisation (HEA 2). Due to the high reactivity of the HfNbTaTiZr composition it has been decided to do perform extra safety testing before developing coatings with the powder of this composition. This powder will then be deposited at a later stage in the project.

2.2 Methodology for coatings deposition and heat treatment

The deposition process parameters employed, for each of the powders in Table 5, to deposit the coatings for this report are the optimised ones as obtained within deliverable D3.2 (for HVOF) and D3.3 (for laser cladding). In this stage, for each material, three types of specimens have been tested for corrosion: one in the as-deposited condition, one in the as-deposited plus heat-treated at condition HT_1 and finally one in the as-deposited plus heat-treated at condition HT_2. Details of these two heat treatments are reported in Tab. 6. Both heat treatments are composed of two steps, where the first one is a dwell at 500 °C for 60 min for both HT_1 and HT_2, performed in order to relax stresses due to coating procedure. The second step is again a dwell, at two different temperatures in the two cases: 900 °C and 1100 °C for HT_1 and HT_2 respectively, in both cases for 60 min. These higher temperatures were selected to impact the coating microstructure and increase the bonding between the substrate and the coated layer by enhancing interdiffusion mechanisms. The furnace was at room temperature (25°C) when the samples were placed in. Argon was flushed during the tests and a natural cooling was employed at the end of the cycle to take the specimens down to room temperature.

Table 6: The two sets of heat treatment parameters (HT_1 and HT_2) used for the experiments.

| Heat treatment | T1 (°C) | HR1 (°C/min) | t1 (min) | T2 (°C) | HR2 (°C/min) | T2 (min) | Cooling type |
|----------------|---------|--------------|----------|---------|--------------|----------|----------------------------|
| HT_1 | 500 | 10 | 60 | 900 | 10 | 60 | Natural furnace atmosphere |
| HT_2 | 500 | 10 | 60 | 1100 | 10 | 60 | Natural furnace atmosphere |

As a result, the overall number of specimens produced is reported in Table 7.

Table 7: Summary of specimens processed for this study

| Specimen name | Deposition technique | Heat treatment type |
|---------------|----------------------|---------------------|
| HVOF_HEA1_HT1 | HVOF | HT_1 |
| HVOF_HEA1_HT2 | HVOF | HT_2 |
| HVOF_HEA2_HT1 | HVOF | HT_1 |
| HVOF_HEA1_HT2 | HVOF | HT_2 |
| HVOF_HEA3_HT1 | HVOF | HT_1 |
| HVOF_HEA3_HT2 | HVOF | HT_2 |
| HVOF_HEA4_HT1 | HVOF | HT_1 |
| HVOF_HEA4_HT2 | HVOF | HT_2 |
| LC_HEA1_HT1 | Laser cladding | HT_1 |
| LC_HEA1_HT2 | Laser cladding | HT_2 |
| LC_HEA2_HT1 | Laser cladding | HT_1 |
| LC_HEA2_HT2 | Laser cladding | HT_2 |
| LC_HEA3_HT1 | Laser cladding | HT_1 |
| LC_HEA3_HT2 | Laser cladding | HT_2 |
| LC_HEA4_HT1 | Laser cladding | HT_1 |
| LC_HEA4_HT2 | Laser cladding | HT_2 |
| LC_HEA5_HT1 | Laser cladding | HT_1 |
| LC_HEA5_HT2 | Laser cladding | HT_2 |

It is worth noting that no HVOF coating made by powder HEA 5 has been produced/tested. This, as explained within deliverable D3.2, is due to the fact that this powder has not been deemed proper for testing within the project due to the poor microstructural properties of the generated coatings. The coatings so produced have been tested for corrosion performance. Phases present within the materials have been analysed both within the powders and within the coatings by means of X-ray diffraction. In this way, possible variations in corrosion resistance could be linked to phase transformations driven by heat treatment.

3. RESULTS

3.1 HEA powders characterisation

The raw elemental powders were processed for high entropy alloys production as described in deliverable D3.2. HEA1 consists of CoCrFeNiMo_{0.85} and it was produced after 210 minute of wet milling in n heptane. We used wet milling to achieve better results regarding the alloying degree. The SEM image and EDS analyses are presented in figure 1. HEA 1 has polygonal shaped particles in the HVOF process required range and from SEM analyses looks homogeneous. HEA 2 was obtained by gas atomisation having spherical particles, very homogenous. HEA 3 was also mechanically alloyed 2 and the composition seems homogenous as the microstructure in figure 1 c reveals. The HEA 4 and HEA 5 followed the mechanical alloying route as HEA 1 and HEA 3 but the parameters were optimised for

each composition. The microstructure for HEA 4 and HEA 5 are homogenous and a certain degree of alloying was obtained.

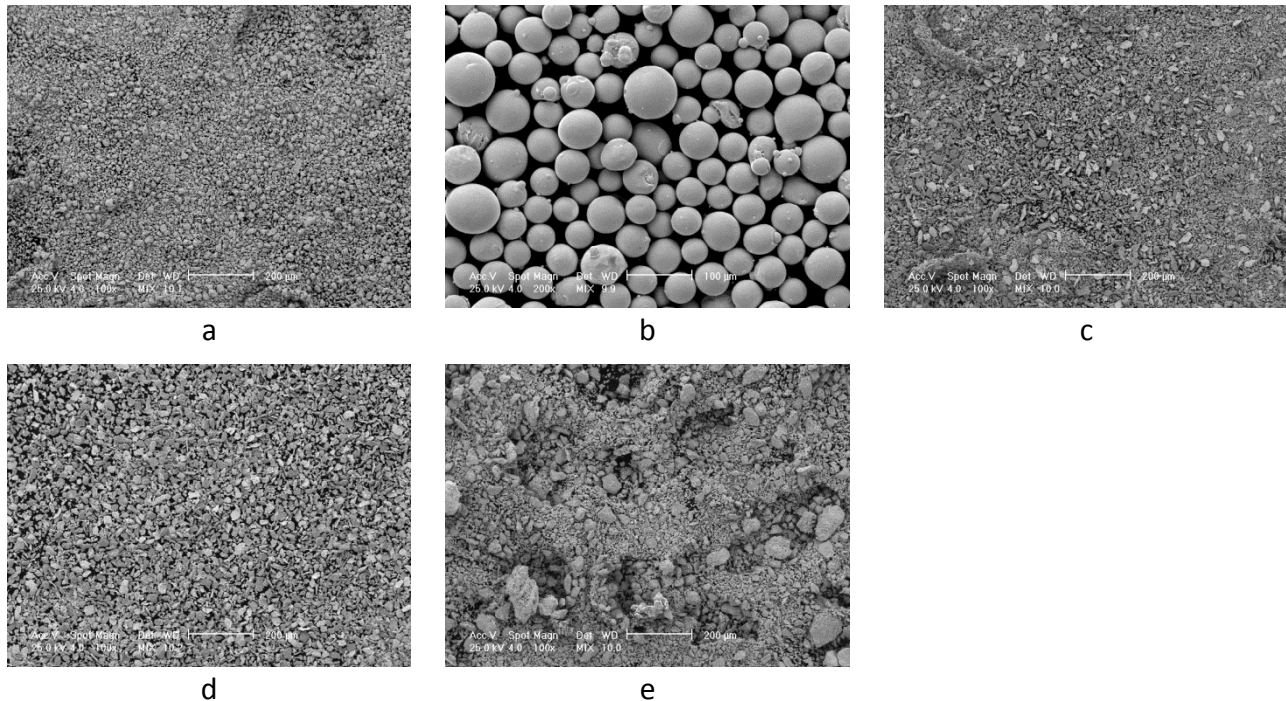


Figure 1 - Microstructures images for HEA 1 (a), HEA 2 (b), HEA 3 (c), HEA 4(d) and HEA 5(e) revealing a homogenous mixture after the alloying time

It has been decided here to select powders HEA1 and HEA2 for the phase evolution discussion from powder to coating, while the only coatings from powder HEA2 are analysed in detail after corrosion. This is for two main reasons: firstly powder HEA1 and HEA2 are, although processed via two different routes, of the same theoretical composition, secondly LMD coatings of powder HEA2 have been demonstrated to perform extremely well in simulated geothermal environment (see deliverable D5.3). Both powders were deposited using two different techniques, high velocity oxygen fuel (HVOF) and laser cladding (LMD). The deposition techniques were described in deliverables D3.2 and D.3.3. For HVOF and LMD we used different size distribution ranges (i.e. cuts) of the powder. The particles dimensions for the HVOF cut were between 20 and 63 μm and for LMD between 63 and 125 μm . The XRD analyses were performed on both cuts to see if the particles dimensions have a strong influence on the alloy present phases.

The XRD for the alloyed powder HEA 1 for LMD and HVOF are presented in the Figure 2.

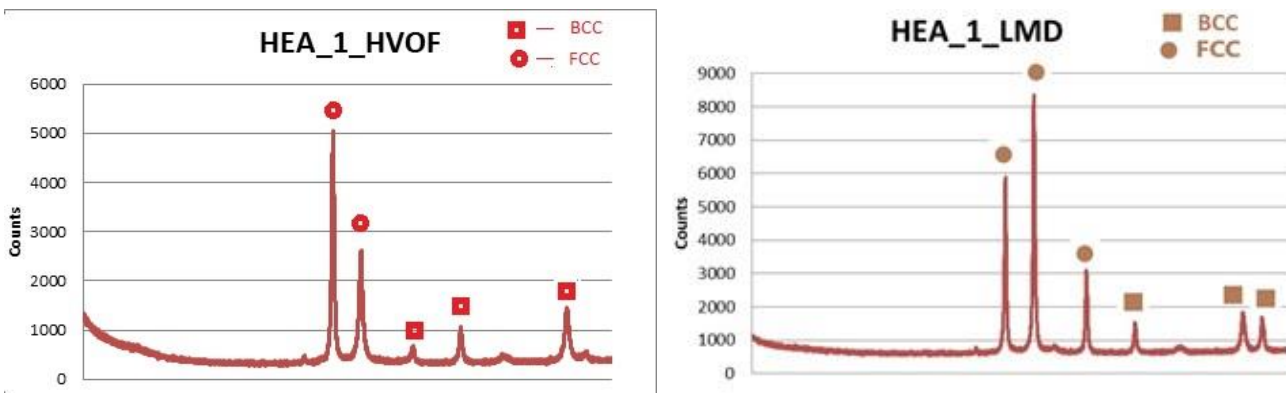


Figure 2. XRD patterns for HEA 1 powder for HVOF and LMD cuts.

The theoretical discussion regarding the valence electron concentration reveals that, for HEA 1 the tendency was to form a mixture of FCC, BCC and σ phases. Usually σ phases appear after exposing the high entropy alloy to high temperature [5] thus meaning that in the powder mixture it is more likely to have a mixture of FCC and BCC phases. During the mechanical alloying process the temperature is considerably lower and this process has a totally different mechanism than for the powder obtained from the gas atomised melt (i.e. HEA2). In the larger cut (i.e. for LMD) the predominant is the FCC phase and for the smaller cut (i.e. for HVOF) the BCC phase seems to be in slightly higher quantity. The dispersed FCC phase can result in strengthening of the particles or can impart special electrical or magnetic properties of the powder. In our case, the main powder property targeted by this producing process was the flowing rate. The flowing rate is a very important parameter for the powder spraying. Our goal is to obtain a flowing rate that allows the powder to be sprayed in optimum condition. The results obtained were very good as detailed in deliverable D3.2.

For HEA 2 the same analyses were performed. The XRD patterns are present in figure 3.

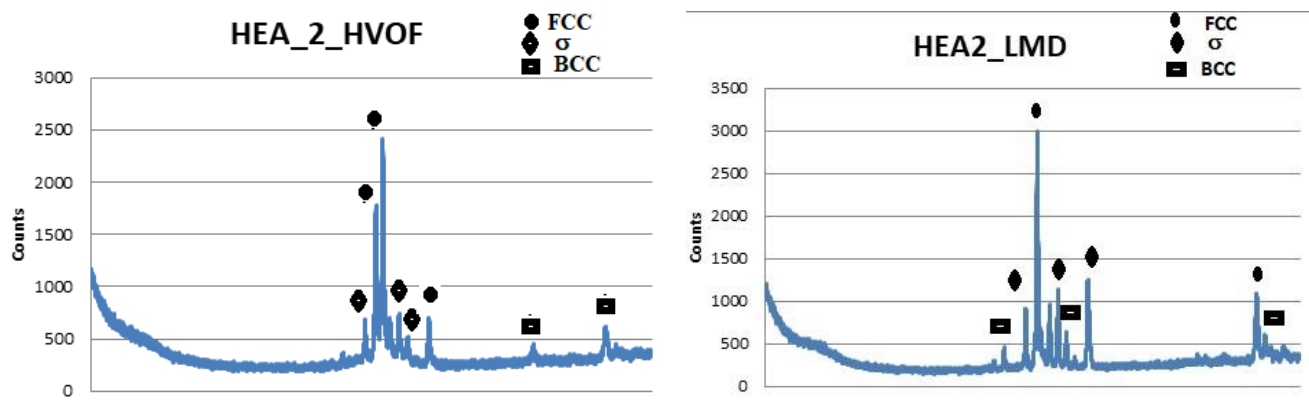


Figure 3. XRD patterns for HEA powder for HVOF and LMD cuts.

For the powder produced by gas atomisation method, the high temperature produced to ensure the raw material melting, made possible the apparition of the σ phase. The σ phase is present in both powder cuts and the phases seems to be distributed relatively homogenous, irrespective of powders dimensions.

The mixture of phases present in the HEA powder match the theoretical calculation that determined VEC=7.8 for this composition. The philosophy of powder producing is different for mechanical alloying and gas atomising. For mechanical alloying, raw powders are placed in a vial with balls and using the mill movement (rotational in our case) the particle weld together and break and then are re-welded again. The process is repeating during the mechanical alloying established time. The distribution of the phases may not be as homogenous as for the powder obtained by gas atomising. In the gas atomised powder each particle is formed of HEA because the raw material are melted together, alloyed and the melt is gas atomised so theoretically each powder particle has the same composition.

A high quality SEM micrograph of one of the powder particle obtained by gas atomising is shown in figure 4 revealing the HEA typical structure. Also, in the same figure, we presented a high quality SEM micrograph of the mechanically alloyed powder, revealing the homogeneous composition of the powder but different structure in comparison to the gas atomized one. The particles are cuboidal in comparison with the spherical one, but, as it was detailed in the deliverable 3.2 the flowing rate calculated for HEA1 and HEA2 were very good, making the powder suitable for spraying.

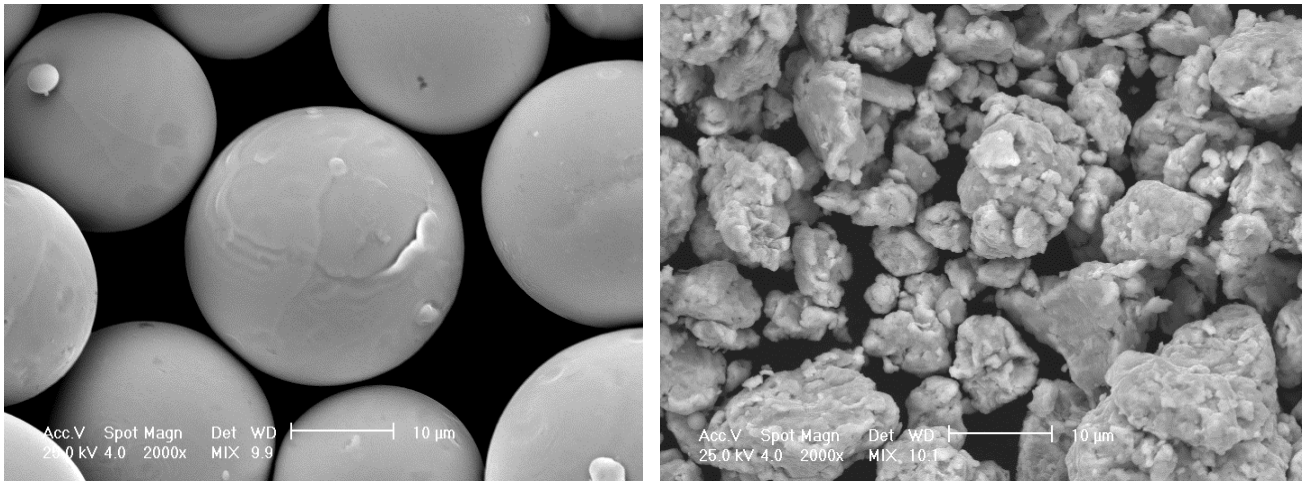


Figure 4. Microstructure at a higher measure revealing the homogeneity of the powder produced by gas atomisation in comparison with the HEA 1 powder produced by mechanical alloying

For HEAs, the terms “solute” and “solvent” lose their conventional meanings, thus the precise contribution of solid-solution strengthening in HEAs remains to be a challenge. Fortunately, Fe, Cr, Ni, Co elements have nearly the same atomic sizes and the mixing enthalpies of different atom-pairs of these four elements are nearly equal to zero. When incorporating Mo elements at a low level to the CoCrFeNi matrix, the element will act as the solute atoms, and Fleisher’s theory [6], a standard model for substitutional solid solution strengthening based on dislocation-solute elastic interactions, could be directly applied to evaluate the potency of solution strengthening caused by the solute atom of Mo [7].

3.2. Performance and characterisation of heat treated coatings

3.2.1. HVOF coatings – characterisation of heat treatment

HVOF coatings have been sprayed with optimised parameters, as described in D3.2. After the corrosion tests the HEA 2 powder behaved better so we will discuss further the coatings performed with HEA 2 powders, heat treated and corroded, to identify the phase changes. The coating was investigated by SEM and the XRD was performed to identify the phases present in the coating.

The HVOF coatings cross section image is presented in figure 5.

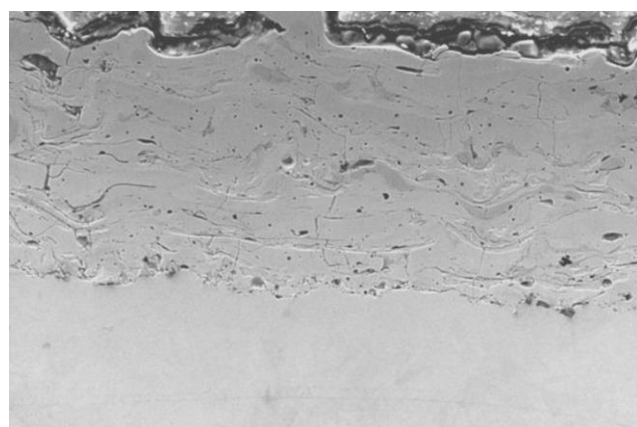


Figure 5. Cross section image for the microstructure of the HVOF coating realized with HEA 2 powder.

The microstructure reveals the homogeneity and the good coating bonding with the substrate. The image reveals multiple phases in the layer. The XRD of the HVOF coating is shown in figure 6.

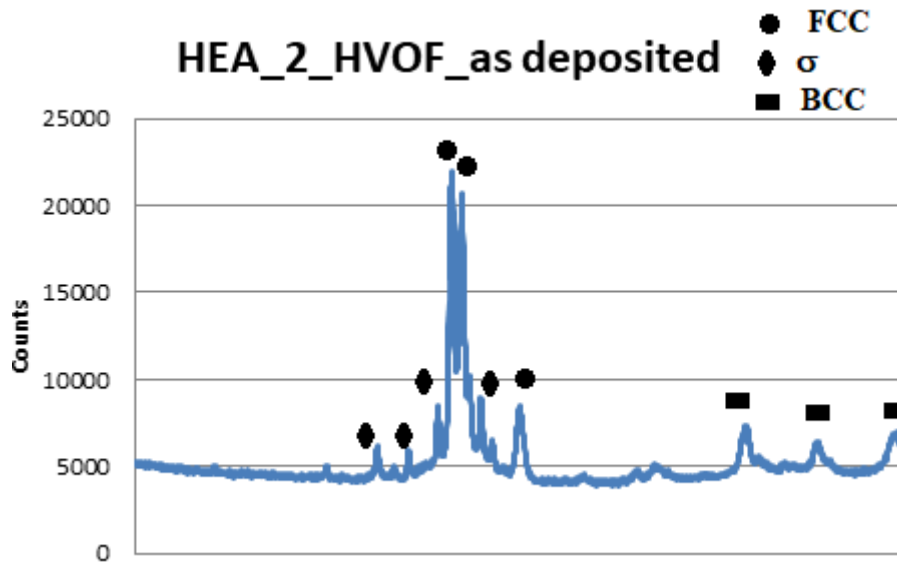


Figure 6. XRD analyses results of the HVOF coating realized with HEA 2 powder.

After the spraying process we can observe that the main FCC peak was broadened and thus could be from the substrate influence. The coatings were realised on carbon steel. The amount of BCC phase slightly decreased and the σ phase is more present in the coating due to the HVOF high temperature during spraying and also rapidly cooling of the coated layer. The XRD profile is quite similar with the HVOF powder cut, but in the coating we can observe a slight peaks broadening.

According to the Gibbs phase rule, $F = C - P + 1$ (where F is the system degree of freedom, C is the number of components, and P is the number of phases), the maximum number of equilibrium phases for an alloy consisting of C components at constant pressure is $P = C + 1$. However, figure 6 highlights that the total number of phases present in the coating is only 2 or 3 which is significantly less than the 6 allowed by the Gibbs phase rule, especially at high temperature. This phenomenon can be attributed to the effect of the high entropy of mixing [8].

The heat treatment was realised for the HVOF samples was realised as described in the methodology section at two temperatures. The heat treated samples were denoted HEA2_HVOF_HT1 and HEA2_HVOF_HT2. The XRD performed on the coating identified the phases present in the heat treated HVOF coating. The XRD for HEA2_HVOF_HT1 and HEA2_HVOF_HT2 samples is shown in figure 7.

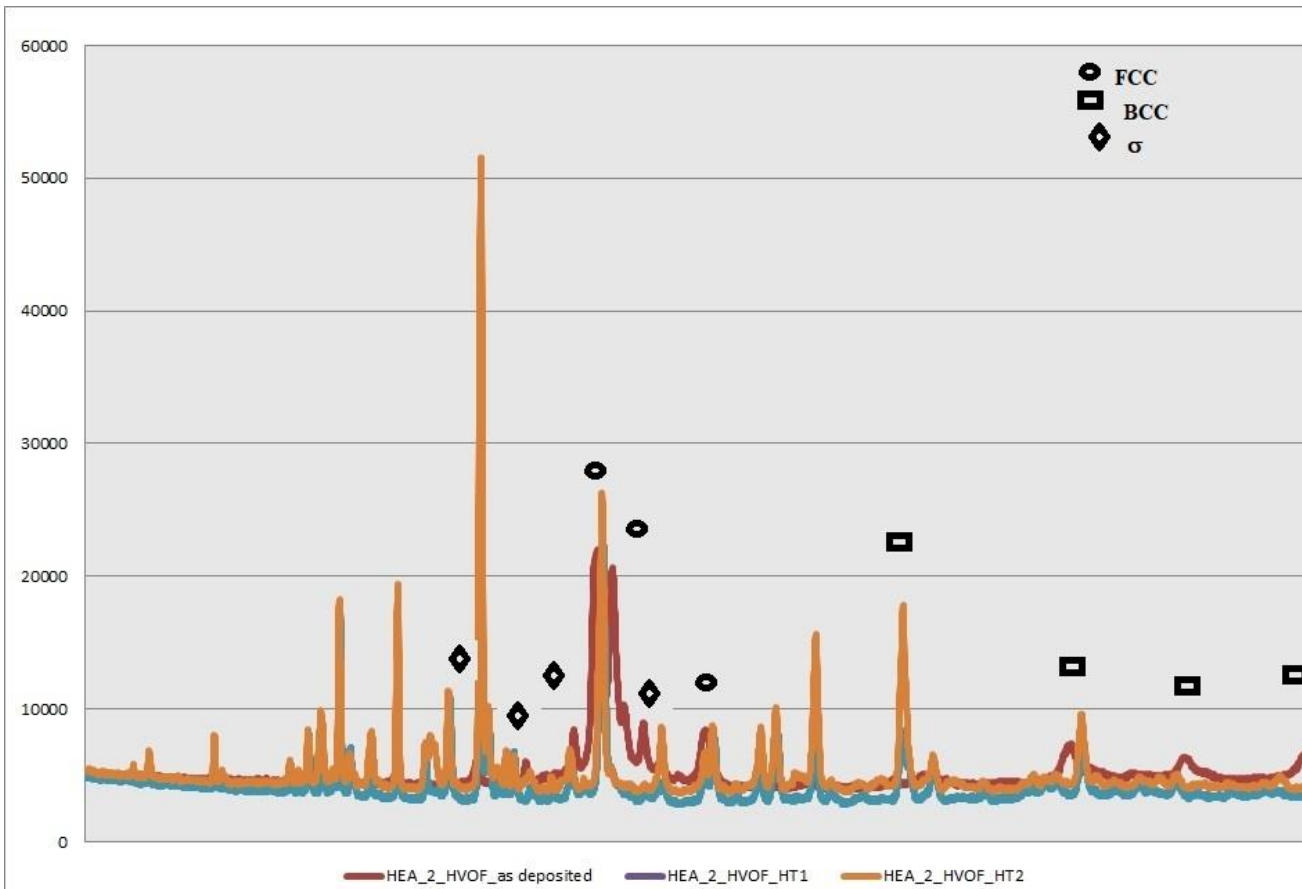


Figure 7. XRD analyses results comparison of the HVOF coating as deposited, heat treated using HT1 and HT2 cycles.

The XRD analyses results revealed that more phases appeared after heat treatment at the higher temperature (1100°C). The as deposited coating and the coating heat treated using HT1 cycle have similar phases, with the difference that the peaks are broadening for the heat treated coating and more σ phases appear into the high entropy coating and less BCC for the coating heat treated using HT1 treatment. For HT2 cycle coating we can clearly see the appearance of more peaks, including a big one, corresponding probably to a FCC peak influence by the substrate. The peaks identification may be difficult but our main goal is to see how the heat treated coating are behaving after corrosion testing and how beneficial is the heat treatment applied to the samples on the corrosion resistance of the coating. The XRD pattern for HT1 coating may be beneficial for the corrosion resistance of the coating.

3.2.2. HVOF coating – Effect of heat treatment on corrosion performance

The samples were subjected to corrosion test as described in the methodology. The corrosion rate for the samples varied as show in graph in the figure 8.

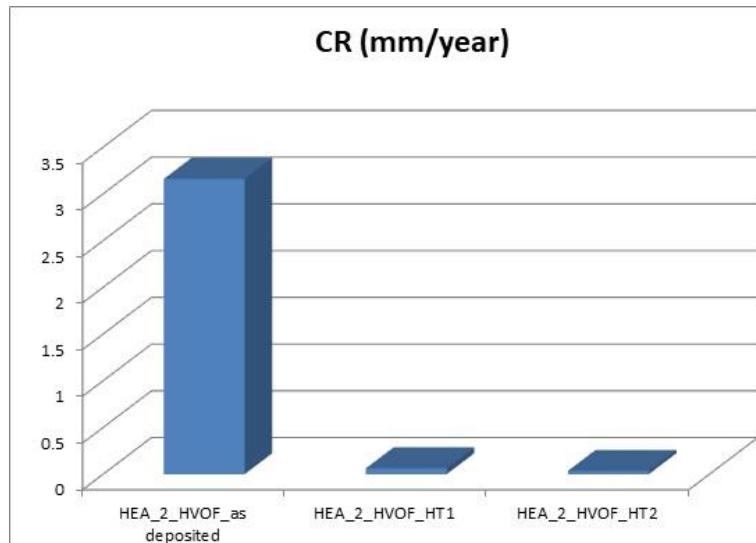


Figure 8. Comparison between the corrosion rate obtained by the samples coated with HEA 2 using HVOF and heat treatment (HT1 and HT2)

The highest value of corrosion rate was obtained for the as deposited coating, CR=3.16 mm/year. The smallest value was obtained for the coating subjected to HT2 cycle. The value of corrosion rate decreased dramatically to 0.036 mm/year proving that the heat treatment applied had a beneficial influence on the HVOF coating. The value obtained for the coating subjected to HT1 is also small, 0.063 mm/year building up the idea that the heat treatment of high entropy HVOF coating could be beneficial due to the good results revealed after corrosion tests.

3.2.3. LMD coatings – characterisation of heat treatment

LMD coatings have been sprayed with optimised parameters, as described in D3.2. After the corrosion tests the HEA 2 powder behaved better so we will discuss further the coatings performed with HEA 2 powders, heat treated and corroded, to identify the phase changes. The coating was investigated by SEM and the XRD was performed to identify the phases present in the coating.

The LMD coatings cross section image is presented in figure 9.

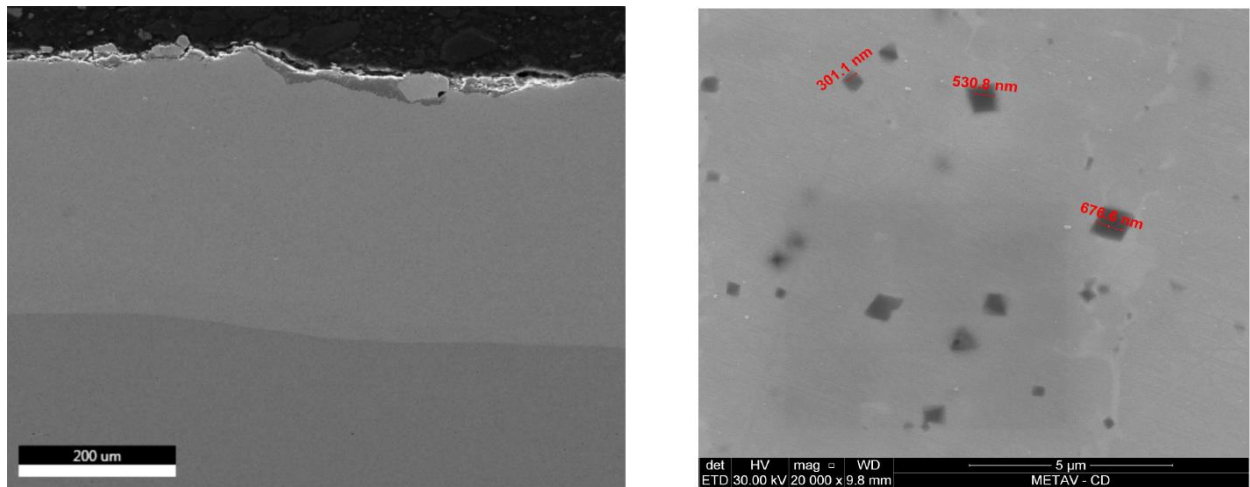


Figure 9. Cross section and top view image for the microstructure of the LMD coating realized with HEA 2 powder.

The microstructure reveals the homogeneity and the good coating bonding with the substrate. The top view reveals a typical FCC high entropy alloy structure. There are some nanometric intermetallic

compounds probably due to Mo present in the HEA 2 composition. Mo is capable of forming hard intermetallic phases with Co, Cr, Fe, and Ni elements. Also, despite their poor plasticity in the bulk state at ambient temperatures, Mo-based intermetallics usually offer an attractive combination of physical and mechanical properties such as good thermal stability, oxidation and wear resistance.

The XRD of the LMD coating is shown in figure 10.

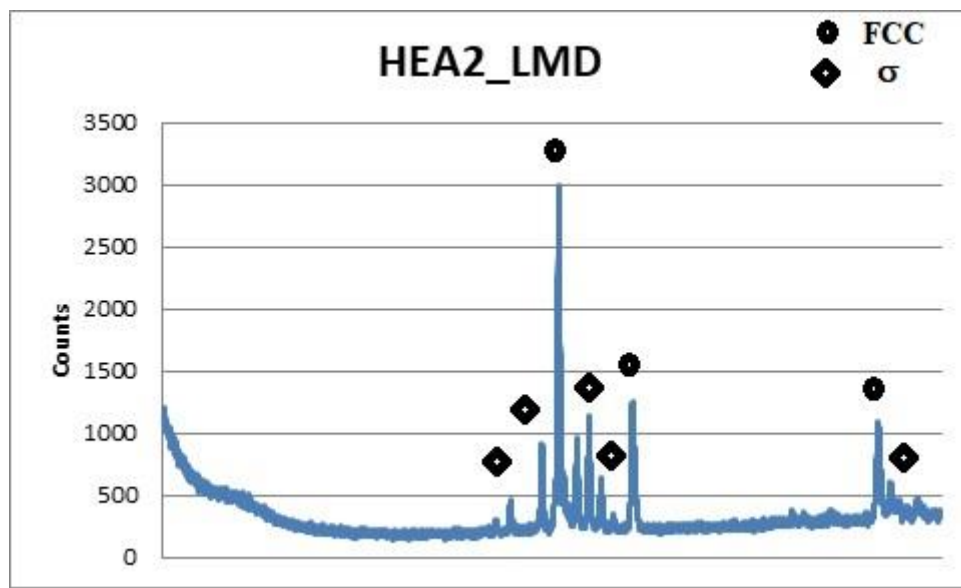


Figure 10. XRD analyses results of the LMD coating realized with HEA 2 powder.

The phases present in the LMD coating seems to be only FCC and σ phase. The process of laser melting deposition tends to stabilise more σ phase than the BCC. The phases formed in HEAs are essentially metastable: they are indeed the firstly formed solid-state phases upon solidification, which are then kept to the ambient temperature due to the sluggish diffusion kinetics of HEAs.

The heat treatment performed for the LMD samples was realised as described in the methodology section at two temperatures. The heat treated samples were denoted HEA2_LMD_HT1 and HEA2_LMD_HT2. The XRD performed on the coating identified the phases present in the heat treated LMD coating. The XRD for HEA2_LMD_HT1 and HEA2_LMD_HT2 samples is shown in figure 11.

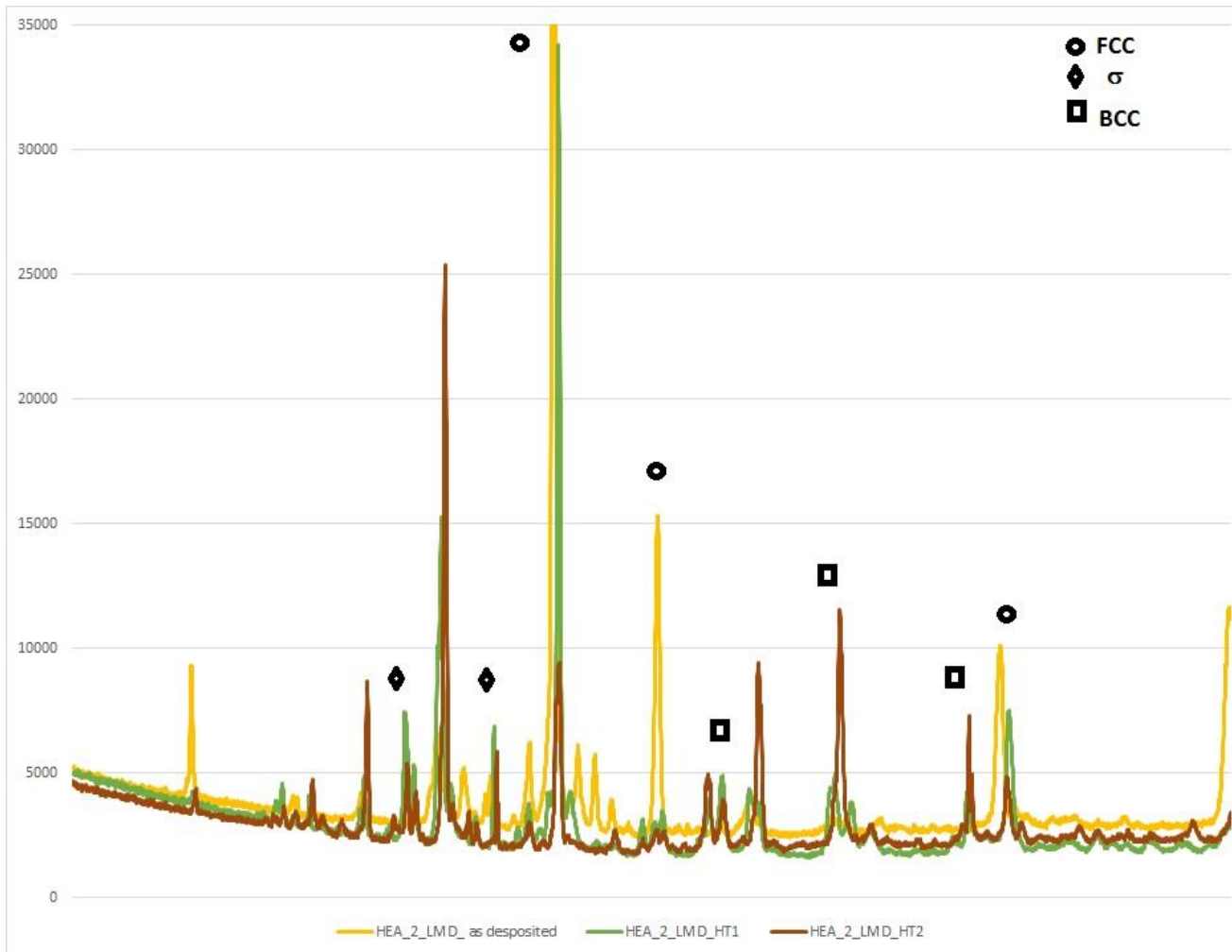


Figure 11. XRD analyses results of the LMD coating realized with HEA 2 powder – comparison between as deposited coating and heat treated using HT1 respectively HT2 cycles.

In comparison with the as deposited coating some BCC phase tends to be present after heat treatment. After the cycle HT2 the coating present a considerably reduced amount of FCC phase and an increase of the σ phase. The BCC phase tends to be stabilised after the heat treatment and is present in the structure after the both heat treatment cycles. The XRD peaks after the second heat treatment are considerably broadened but after the first heat treatment the broadening effect is not so pronounced.

3.2.4. LMD coatings – effect of heat treatment on corrosion performance

The samples were subjected to corrosion test as described in the methodology. The corrosion rate for the samples varied as show in graph in the figure 12.

The highest value of corrosion rate was obtained for the HEA_2_LMD-HT2, meaning the coating subjected to the second cycle of heat treatment, HT2. The smallest value was obtained for the as deposited coating, CR=0.09 mm/year. In comparison with the HVOF coating the heat treatment cycle seems to produce a negative effect on the laser melting deposition coating.

The corrosion rate for the first heat treatment cycle, HT1 dramatically increased, as it can be seen on the graph presented in figure 12 and the effect is more visible on the sample subjected to the second heat treatment cycle. The conclusion would be that the heat treatment has a detrimental effect on the HEA LMD coatings.

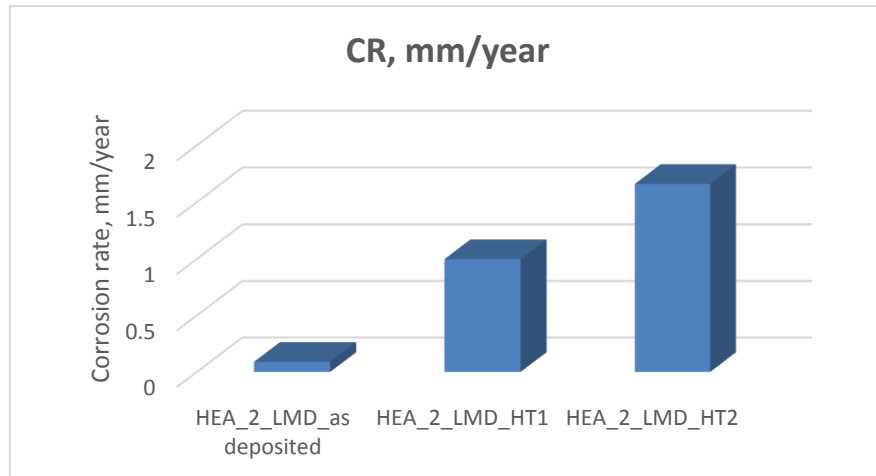


Figure 12. Comparison between the corrosion rate obtained by the samples coated with HEA 2 using LMD and heat treatment (HT1 and HT2)

4. DISCUSSION – PHASE EVOLUTION DURING HEAT TREATMENT

The formation of FCC phase is promoted when most of the binary constituents crystallize in FCC structure. The binary constituents in CoCrFeNiMo_x alloy, namely, CoNi, CoFe, FeNi, all have FCC structure and hence stabilize this phase. Co is HCP at room temperature and it transforms to FCC above 450° C and is easily accommodated in the parent FeNi structure (FCC). FCC structure which can be attributed to the presence of other three FCC elements (Co and Ni). Complete solubility of Co-Ni, sufficient solubility of Fe in Ni stabilize the FCC structure in these alloys. Hence, whenever these elements are present together, we are more likely to get a FCC HEA. Equiatomic alloys such as CoCrFeNi [5] and CoCrFeMnNi [9] are important FCC alloys which predominantly exhibit a single-phase FCC structure. Here all the constituent elements are similar in sizes, valences, and electronegativity. However, the unique properties of HEAs lies in the fact that even elements of different crystal structure might combine to form a single phase solid solution. For example, in CoCrFeNi and CoCrFeMnNi alloys, not all the elements have FCC structure at room temperature, yet the alloys exhibit a single-phase structure. This non-conformance to Hume-Rothery rules in multicomponent system is, because the phase evolution in HEAs, largely dominated by the binary constituent with highest driving force of formation. High-entropy effect enhancing the mixing of elements also has an important contribution. There is a high possibility that FCC HEAs generally have low-stacking fault energy and tend to have fine stable grain structure after heat treatment. Non-equilibrium processing route is probably more likely to give rise to single phase. Most HEAs that show the presence of more than two phases are processed through liquid processing techniques, as vacuum arc melting. The solidification rate in these processes is sometimes slow and allows sufficient time for different phases to grow or for elemental segregation. When some elements have large positive mixing enthalpy in the interactions with other elements might occur strong elemental segregations. BCC HEAs are important in high-strength applications as they usually show better mechanical properties like higher yield strength than FCC HEAs. Formation of BCC structure is favoured when most of the binary pairs present in the alloy crystallize in BCC lattice. Phase formation in HEAs appears to be governed more by the binary constituent pairs which evolve first rather than the individual elements themselves. HEAs of refractory elements have been synthesized and are shown to have single-phase BCC structure in the as-cast state. For the composition CoCrFeNiMo_{0.85} the binary pairs have the following distribution: CoNi, NiCr, NiFe, NiMo have FCC structure, CoCr, NiMo, FeCr and FeMo have σ phase and CoFe and CrMo have BCC structure. The number of FCC binary pairs and σ phase are equal for this alloy fact that

is reflected in LMD coatings (as deposited). The LMD process could be compared with liquid-phase processing. The spraying using HVOF process induce some BCC phase probably due to the higher temperature present in the torch. The formation of single phase is attributed to the conformance of individual elements to Hume-Rothery rules. Mo, Nb, Ta, V, and W have similar atomic radii, valence, and BCC crystal structure. It can be summarized that individual elements promoting BCC phase formation are Al, Cr, Fe, Ti, Mo, Nb, Ta, V, and W. Al is unique because it has a FCC structure. It has been shown that Al stabilizes FCC structure when its concentration is less than 11 at.% and promotes BCC phase formation when present in a greater amount [9]. This is because, although Al has a FCC structure, many of its binary compounds AlNi, AlFe, AlCo, AlTi) crystallize in BCC lattice due to the formation of d_p hybrid orbital. Cr, Fe, Mo, Nb, Ta, V, and W have BCC structure at room temperature and hence tend to stabilize BCC structure in HEAs. It should be mentioned that phase type prediction is done in a qualitative manner from constituent-element's features and/or unlike-atomic pair's features, which is similar to Hume-Rothery rules. While it is comprehensive, it is not possible to make an accurate prediction. This is simply because HEAs involve multi-elements and many unlike atomic pairs. As a result, various quantitative ways using parameters such as mixing entropy, mixing enthalpy, atomic size difference, and valence electron concentration are proposed for the prediction. The σ phase is usually observed in Cr-containing steels and has a typical composition of equiatomic FeCr with a tetragonal structure. The σ phase has also been observed with equiatomic CoCr or FeMo in binary CoCr and FeMo alloys. A large number of HEAs containing Fe and/or Co together with higher amounts of Cr and/or Mo have shown the formation of σ phase at various stages of their processing. In HEAs, the σ phase is also a multicomponent solid solution. The formation of σ phase is an indication that different types of solid solutions in HEAs could form depending on the interaction and atomic size difference between elements and not just the configurational entropy alone. The σ phase is in fact a topologically close-packed phase in which components with larger atomic size occupy one specific set of lattice sites while smaller atoms occupy another set so as to get a higher number of bonding to lower its overall free energy, although their interactions (or enthalpy of mixing) between components are small. Addition of molybdenum tends to stabilize the formation of a BCC structure and/or appearance of σ phase. Formation of σ phase has also been reported in CoCrFeNiMo_x alloys with increasing Mo content [9]. Increasing Mo content has also been shown to transform the cast structure to a eutectic structure. When added to AlCrFeNi alloys, Mo dissolves preferentially in the (Fe,Cr)-rich BCC phase while the other BCC phase, based on Al_Ni is lean in Mo [10]. Increase in Mo content transforms the eutectic microstructure to hypo/hyper eutectic structure. This preference is probably due to higher driving force for the formation of a stable σ phase of FeCrMo type. Cr is an important constituent in HEAs, and as already discussed in the context of equiatomic alloys, Cr stabilizes the BCC structure and promotes formation of the σ phase particularly in presence of Fe, Co, and Ni. When temperature is increased the σ phase tends to be transformed in BCC phase and the structure receive different properties. For HVOF coating the balanced phase's composition with more BCC and FCC resulted in an improved corrosion resistance for the heat treated coatings. For the LMD coatings, the σ phase stabilised by the Cr presence together with Co, Fe and Ni has a good influence on the coating as deposited and a detrimental influence after heat treatment.

In figure 13 a comparison between the XRD taken after corrosion is for the as deposited coating, HT1 cycle heat treated and HT2 cycle heat treated coating is presented.

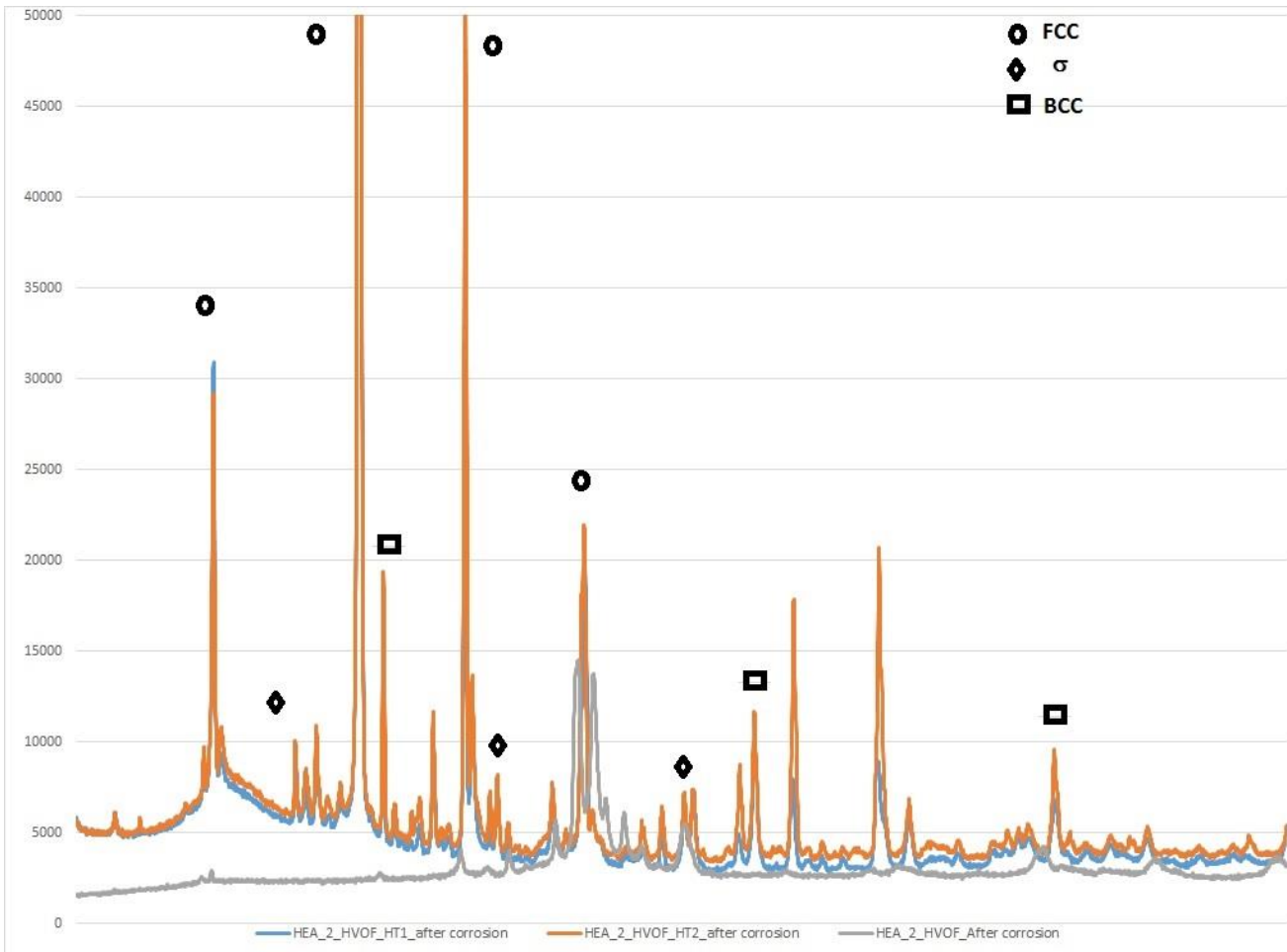


Figure 13. XRD analyses results of the HVOF coating realized with HEA 2 powder – comparison between as deposited coating and heat treated using HT1 respectively HT2 cycles.

Figure 13 is in accordance with the previous discussion revealing the FCC predominant phase for the HEA_2_HVOF_HT2 coating promoting an increased resistance to corrosion for this coating. In figure 14 we can observe the comparison for LMD coatings, also using HEA_2 composition and HT1 heat treatment cycle and HT2 heat treatment cycle. The other unindexed peaks may come from the corrosion film and they are difficult to be identified.

The peaks for the HEA_2_LMD_as deposited coating match in a certain extent the pattern of the high entropy alloy as deposited meaning that the coating was not so corroded and reveals a better behaviour to corrosion then the heat treated samples matching our supposition revealed in the discussion section. The BCC phase appearance in the LMD coating induced some stresses that reduced the coating corrosion resistance meaning that, for LMD coating, heat treatment is detrimental for corrosion resistance results.

Document: D3.6 : Scientific study on the passive film and heat treatment on corrosion behaviour of HEAs
Version: 01
Date: 31 July 2019

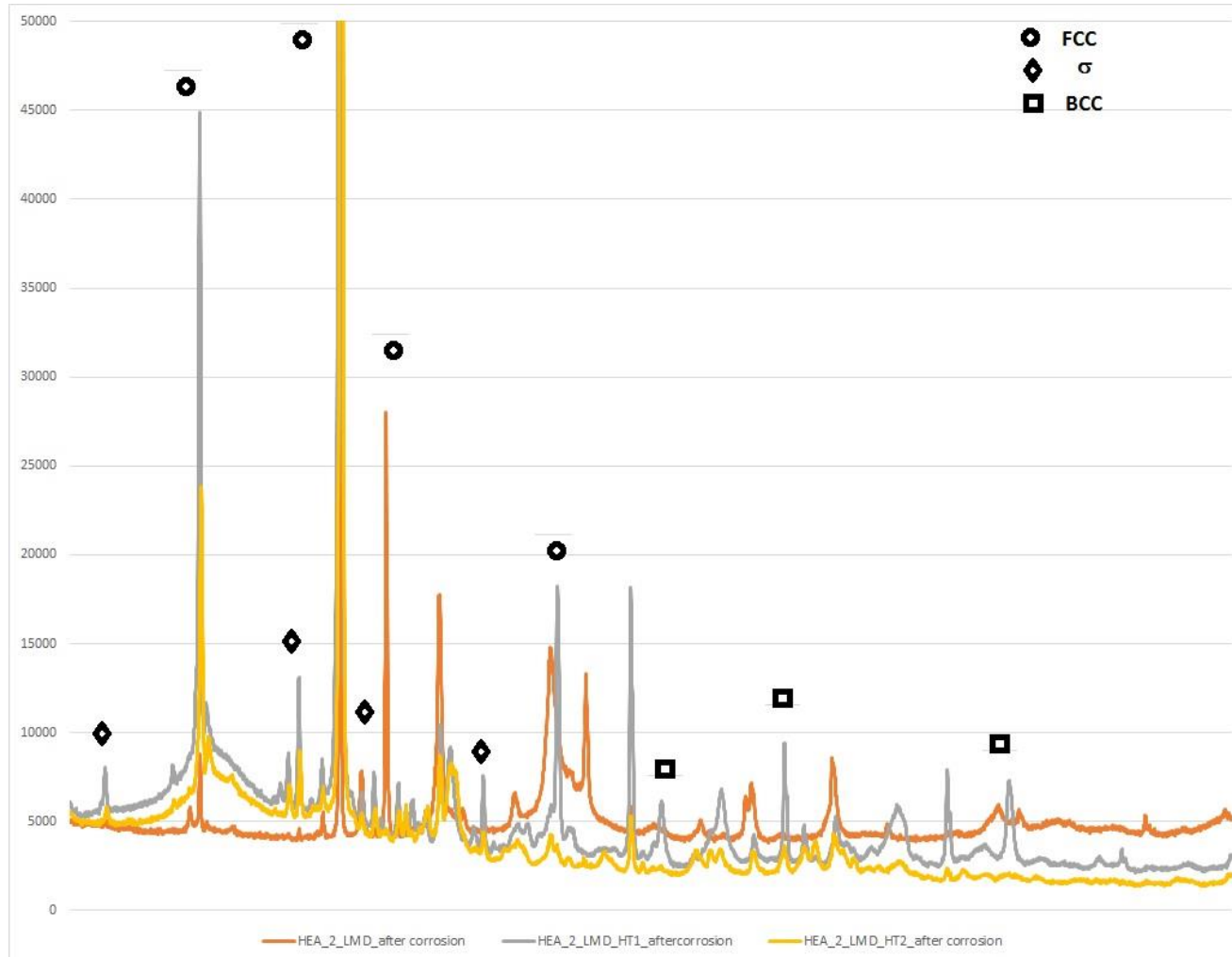


Figure 14. XRD analyses results of the LMD coating realized with HEA 2 powder – comparison between as deposited coating and heat treated using HT1 respectively HT2 cycles.

5. CONCLUSIONS

In this deliverable we presented all the theoretical calculation realised in order to choose the most suitable high-entropy alloy (HEA) composition for the purpose of the Geo-Coat project. In this way, we selected 6 promising candidates. The powder produced were characterised and the phases presented in each composition were identified. Phase modifications has then been followed after heat treatment and corrosion testing of the coatings via XRD analysis.

For HVOF-HEA2 coatings, we could observe the presence of FCC, BCC and σ phase. After heat treatment cycle 2 (HT2) the amount of BCC phase decreased and the σ phase amount increased, with a corresponding increase in corrosion resistance of the coating. It was in fact demonstrated that, for HVOF coatings, the heat treatment cycles were in all cases beneficial

For the coating realised using laser melting deposition (LMD) the heat treatment cycles proved to be detrimental to corrosion resistance. The phase evolution was discussed and it was confirmed that the addition of molybdenum tends to stabilize the formation of a BCC structure and/or appearance of an σ phase. The σ phase presence in the high entropy alloy seems to influence in a good way the corrosion behaviour.

Overall, the study realised on the phases evolution of the high entropy alloy coating confirmed that the heat treatment was beneficial for HVOF coating and detrimental for LMD coatings.

REFERENCES

- [1] I. Csaki, S.N. Karlsdottir, R. Stefanoiu, L.E. Geambazu, Corrosion behaviour in geothermal steam of CoCrFeNiMo high entropy alloy, NACE 2018, Phoenix, Arizona
- [2] Y. Zhang, Y. J. Zhou, J. P. Lin, G. L. Chen, and P. K. Liaw, Adv. Eng. Mater. 10, 534 (2008).
- [3] S. Guo, C. Ng, J. Lu, C.T. Liu, Effect of valence electron concentration on stability of fcc or bcc phase in high entropy alloys”, J Appl Phys. 109 (2011) 1–6
- [4] A. Takeuchi, A. Inoue, Mater. Trans. JIM 46 (2005) 2817–2829
- [5] Shun, T.T.; Chang, L.Y.; Shiu, M.H. Microstructure and mechanical properties of multiprincipal component CoCrFeNiMox alloys, Mater. Charact. 2012, 70, 63–67
- [6] R.L. Fleischer, Substitutional solution hardening, Acta Metall. 11 (1963) pp. 203-209
- [7] 1. Liu, W.H.; Lu, Z.P.; He, J.Y.; Luan, J.H.; Wang, Z.J.; Liu, B.; Liu, Y.; Chen, M.W.; Liu, C.T. Ductile CoCrFeNiMox high entropy alloys strengthened by hard intermetallic phases, Acta Materialia 2016, 116, 332-342
- [8] Yeh JW, Chen SK, Gan JY, Chin TS, Shun TT, Tsau CH, et al. Nanostructured high-entropy alloys with multi-principal elements: novel alloy design concepts and outcomes. Adv Eng Mater2004; 6(5):299–303.
- [9] Liu, W.H., Wu, Y., He, J.Y., Nieh, T.G., Lu, Z.P., 2013. Grain growth and the Hall-Petch relationship in a high-entropy FeCrNiCoMn alloy. Scr. Mater. 68, 526-529.
- [10] Zhu, J.M., Fu, H.M., Zhang, H.F., Wang, A.M., Li, H., Hu, Z.Q., 2010a. Microstructures and compressive properties of multicomponent AlCoCrFeNiMox alloys. Mater. Sci. Eng. A 527, 6975 - 6979.